NANO LETTERS
Letter
pubs.acs.org/NanoLett

Wireless Communication with Nanoplasmonic Data Carriers: Macroscale Propagation of Nanophotonic Plasmon Polaritons Probed by Near-Field Nanoimaging

Moshik Cohen,[*,†,§] Yossi Abulafia,[§] Dmitry Lev,[∥] Aaron Lewis,[∥] Reuven Shavit,[‡] and Zeev Zalevsky[†,§]

[†]Faculty of Engineering, Bar-Ilan University, Ramat-Gan 52900, Israel
[‡]Department of Electrical and Computer Engineering, Ben-Gurion University of the Negev, Beer-Sheva 84105, Israel
[§]Bar-Ilan Institute for Nanotechnology & Advanced Materials, Ramat-Gan 52900, Israel
[∥]Department of Applied Physics, Selim and Rachel Benin School of Engineering and Computer Science, The Hebrew University, Givat Ram, Jerusalem 9190401, Israel

ABSTRACT: The ability to control the energy flow of light at the nanoscale is fundamental to modern communication and big-data technologies, as well as quantum information processing schemes. However, because photons are diffraction-limited, efforts of confining them to dimensions of integrated electronics have so far proven elusive. A promising way to facilitate nanoscale manipulation of light is through plasmon polaritons—coupled excitations of photons and charge carriers. These tightly confined hybrid waves can facilitate compression of optical functionalities to the nanoscale but suffer from huge propagation losses that limit their use to mostly subwavelength scale applications. With only weak evidence of macroscale plasmon polaritons, propagation has recently been reported theoretically and indirectly, no experiments so far have directly resolved long-range propagating optical plasmon polaritons in real space. Here, we launch and detect nanoscale optical signals, for record distances in a wireless link based on novel plasmonic nanotransceivers. We use a combination of scanning probe microscopies to provide high resolution real space images of the optical near fields and investigate the long-range propagation of nanoscales optical signals. We design our nanotransceivers based on a high-performance nanoantenna, *Plantenna*, hybridized with channel plasmon waveguides with a cross-section of 20 nm × 20 nm, and observe propagation for distances up to 1000 times greater than the plasmon wavelength. We experimentally show that our approach hugely outperforms both waveguide and wireless nanophotonic links. This successful alliance between Plantenna and channel plasmon waveguides paves the way for new generations of optical interconnects and expedites long-range interaction between quantum emitters and photomolecular devices.

KEYWORDS: *Plasmonics, nanoantennas, channel waveguides, wireless, nanoimaging*

The proposed scheme is designed to enable macroscale communication between nanoscale devices utilizing surface plasmon polaritons (SPPs). Hence, we use channel waveguides that confine SPPs to their channel dimensions, which can be as small as several nanometers.[1−8] However, as dimensions decrease, SPPs exhibit increased losses that limit their propagation in waveguides to distances of only few micrometers. To address this fundamental limitation, we convert channel SPPs to optical surface waves that propagate for significantly larger distances on dielectric substrates. A high-efficiency nanoreceiver, designed to convert surface waves to channel SPPs, is placed the remote edge of the system. Figure 1a illustrates the proposed communication nanosystem, which (a) converts light to nanoscale SPPs, (b) propagates SPPs in channel waveguide, (c) converts these SPPs to surface waves and propagatea them for long distance, and (d) excites SPPs from the surface waves at remote locations. As shown in the right-hand side of Figure 1a, laser light illuminates the *Plantenna* to launch SPPs at the waveguide. Second, Plantenna, located at the other edge of the waveguide, converts these SPPs to surface waves that propagate on the substrate. The surface waves are reconverted to SPPs at a remote, Plantenna based nanoreceiver. We use waveguides with a propagation loss of $e^{-\alpha l}$, where the absorption constant α = (18 μm)$^{-1}$ for a channel width of 20 nm at a red wavelength of λ = 633 nm and l is the propagation length.

In contrast, absorption for wireless links occur only at the antennas and are much lower than for a waveguide. For conventional (e.g., dipole, bowtie) nanoantennas, the propagation loss for wireless links behaves like $(D/l)^2$, where D is the directivity.[9] Here, we show that Plantenna based wireless links hugely outperform both waveguide and conventional nanoantenna based alternatives. Figure 1b presents a 3D model of the nanotransceiver, with zoom in to the Plantenna region

Received: January 19, 2017
Revised: April 25, 2017
Published: May 3, 2017

DOI: 10.1021/acs.nanolett.7b00266
Nano Lett. XXXX, XXX, XXX−XXX

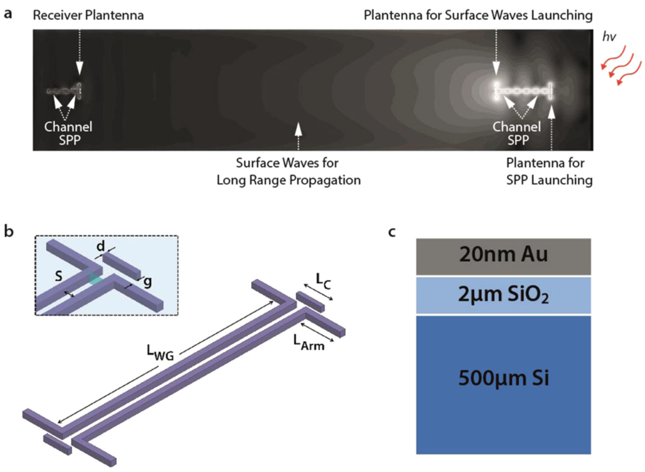

Figure 1. Wireless communications with optical plasmon polaritons. (a) Illustration of the proposed nanoscale communication system. SPP launching Plantenna (right) converts free space light to propagating waveguides SPPs, which are coupled to surface waves by the "Surface Waves Launching Plantenna" for long-range propagation. A Plantenna based nanoreceiver (left) converts the surface waves to channel SPPS at remote distances. (b) 3D model of a Plantenna based plasmonic nanotransceiver. Zoom in to the Plantenna region is shown in the inset c, materials stack up used to fabricate the devices.

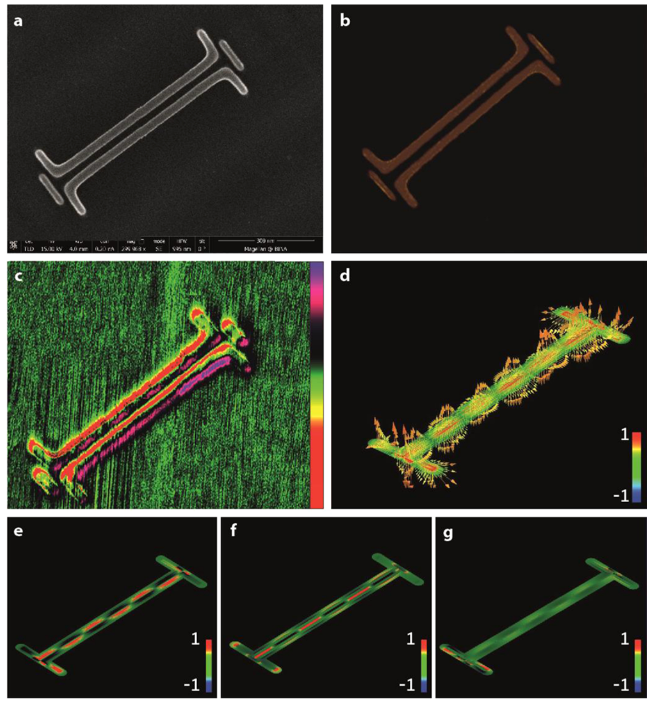

Figure 2. Plantenna-based plasmonic nanotransceiver. (a) High-resolution SEM image of the fabricated nanotransceiver. (b) 3D AFM image of the fabricated nanotransceiver. (c) KPFM under optical illumination analysis of the nanotransceiver. KPFM signal scale bar: ±4.7 V. (d) Numerically calculated optical near-field vector. (e) Numerically calculated optical near-field image showing $\mathrm{Re}(E_z) = |E_z| \cos(\phi_z)$. (f) Numerically calculated optical near-field showing $\mathrm{Re}(E_x)$. (g) Numerically calculated optical near field showing $\mathrm{Re}(E_y)$. Scale bar: 100 nm.

shown in the inset. The physical principle behind the Plantenna invention is the enormous field enhancement and confinement exhibited by resonant, optically illuminated adjacent metallic nanoparticles. These properties, mainly originated from coherent capacitive coupling between the particles, are significantly better than those of isolated nanoparticles. The Plantenna comprised of two metallic nanorods of length L_{Arm}, separated by a nanoscopic gap (s = 10−35 nm), in a dipole arrangement. An additional nanorod, termed director, is placed at much closer proximity of only 7 nm ($g \sim 7$ nm) to the dipole. A detailed analysis on the Plantenna physics, which also includes optimization for high efficiency excitation of channel SPPs, was recently reported.[5] Figure 1c shows the material stack up used in this work, comprised of 20 nm Au layer deposited on a Si on insulator (SOI) wafer (500 μm Si, 2 μm SiO_2), for potential CMOS computability.

For nanofabrication, we use electron beam lithography (EBL), ion beam sputtering (Au, 20 nm), and liftoff. After liftoff, the resist is completely removed, allowing contact mode near-field optical characterization. We fabricated devices comprised of standalone nanotransceivers and complete communication systems. Figure 2a shows a high-resolution scanning electron microscopy (HR-SEM) image of a fabricated nanotransceiver, recorded at beam current of 0.4 nA and low accelerating voltage of 5 kV, for sub 1 nm imaging resolution; corresponding 3D AFM topography is shown in Figure 2b. Nanotransceivers with dimensions of L_{Arm} = 220 nm, L_{C} = 120 nm, s = 20 nm, g = 7 nm, and L_{WG} = 1.5 μm were fabricated successfully and repeatedly. Figure 2c shows near-field KPFM nanoimaging under illumination with a He−Ne laser (λ_0 = 633 nm), recorded at a set lift height of 30 nm using a high aspect ratio uncoated Si AFM tip with a diameter of 2 nm. As observed, the laser light is efficiently converted to propagating plasmons at the waveguide channel by the Rx (right) Plantenna and then recoupled to surface waves via the Tx (left) Plantenna. Characterized by periodic peaks (purple) in the KPFM signal imaged at the waveguide channel, SPPs with an effective wavelength of 35−150 nm were measured. The experimental results are reproduced by numerical calculation results, presented at the optical frequency of 474 THz (633 nm). The theoretical results are obtained using a high-frequency structure simulator based on the finite element method (FEM).[3−5,10,11] Numerical calculation results of the device are shown in Figure 2d−g, with Figure 2d showing the local near-field vector in 3D, and Figure 2e−g presenting the scalar component of the electrical near-field magnitudes $\mathrm{Re}\{|E_z|\}$, $\mathrm{Re}\{|E_x|\}$, and $\mathrm{Re}\{|E_y|\}$, respectively.

The analysis of a nanoscale wireless communication system that transmits and receives optical plasmon polaritons with a cross section of 20 nm × 20 nm to distance of 12 μm is shown in Figure 3. The system is comprised of a plasmonic nanotransceiver (Figure 1b) and a nanoplasmonic receiver, separated by a distance of 12 μm. Figure 3a presents 3D AFM topography mapping of the nanosystem, where the transceiver is fabricated at the right-hand side and the receiver is located at the left side. To image the near-field structure of long-range plasmon polaritons transfer in real space, we use a combination of KPFM and SNOM. KPFM enables near-field mapping of plasmonic devices with a very high resolution. However, it has limited efficiency in characterizing dielectric devices, mainly since the work function of dielectric materials barely can be modified by optical illumination.[3,4,6,12] Figure 3b shows KPFM analysis of the nanosystem, illuminated by a He−Ne laser (λ = 633 m), linearly polarized in parallel to the dipole orientation and focused to diameter of 700 nm. Channel SPPs are observed at the nanotransceiver channel waveguide, propagate for

DOI: 10.1021/acs.nanolett.7b00266
Nano Lett. XXXX, XXX, XXX−XXX

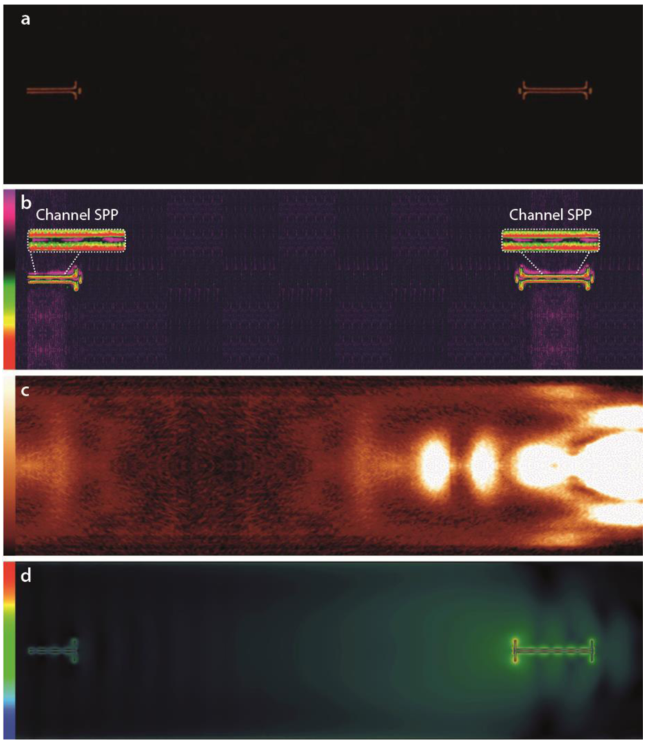

Figure 3. Characterization of the proposed wireless link, demonstrating efficient long-range propagation of tightly confined optical plasmon polaritons. (a) 3D AFM image of the fabricated wireless link system. (b) KPFM under optical illumination analysis of the wireless link system, showing SPPs at the transmission (right) and reception (left) sides; inset—zoom in to the respective waveguide channel. KPFM signal scale bar: ±4.7 V. (c) SNOM analysis of the wireless link system, showing SPPs at the transmission (right) and reception (left) sides, as well as the coupling to surface waves that enable the long-range propagation. (d) Numerically calculated near-field image, showing the complete optical wireless transfer link. Scale bar: 750 nm.

distance of $L_{WG} = 1\ \mu$m, followed by strong "hot spot" at the Tx Plantenna that converts them to surface waves. A zoom in to the channel region is presented in the inset, clearly showing the periodic structure of the excited SPPs. Remarkably, pronounced SPP excitation is observed at the distanced receiver, which is not illuminated by the laser. Highlighted in the left inset, the channel SPPs at the receiver waveguide are excited by efficient coupling of surface waves to SPP by the receiver Plantenna. The surface waves on the SiO_2 surface are imaged in the near field via SNOM, as shown in Figure 3c. Naturally, SNOM provides lower resolution images compared to KPFM;[3] however, its direct optical imaging mechanism enables mapping of the surface photons that propagate on the dielectric medium, unlike KPFM. Note that the SNOM image exhibits high intensity at the physical locations of the transceiver and receiver, originated by plasmon excitation. Hence, we state that the combination of KPFM and SNOM provides a complementary, complete real-space nanoimaging approach for the characterization of nanoscale wireless communication systems, which facilitates high-resolution nanoimaging of both plasmons and optical surface waves. Numerical calculation results of the nanosystem, presenting the electric near-field magnitude |**E**|, are shown in Figure 3d. Both channel SPPs as well as the surface waves in the dielectric substrate are clearly captured, providing additional confirmation to our approach.

To unambiguously demonstrate the excellent efficiency of our Plantenna based nanosystem, we compare its performances to direct channel waveguiding link[6−8,13] and to wireless link based on dipole nanoantennas.[14−17] For the wireless link configurations (Figure 4a−d) the distance between the transceiver and receiver is 10 μm, and for the direct link (e.g., Figure 4e−f) the waveguide length is 3 μm, limited by fabrication constraints. Figure 4a shows AFM image of our proposed Plantenna based nanosystem, as the corresponding KPFM mapping is shown in Figure 4b with a voltage scale bar of ±4.7 V. Pronounced plasmon excitation is probed at the receiver, evidenced by the modal structure of the field inside

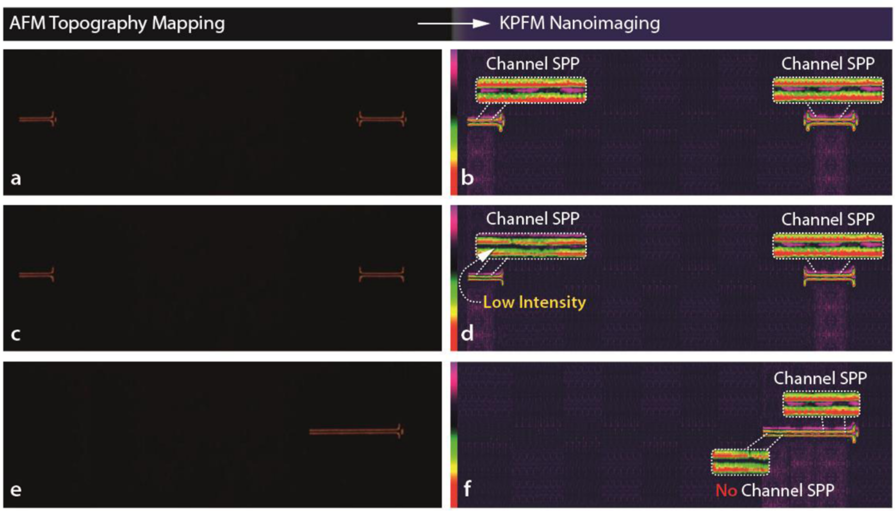

Figure 4. Comparison between nanophotonic links. (a) 3D AFM image of the Plantenna-based wireless link system. (b) KPFM under optical illumination analysis of the Plantenna-based wireless link system; KPFM signal scale bar: ±4.7 V. (c) 3D AFM image of the dipole nanoantenna-based wireless link system. (d) KPFM under optical illumination analysis of the dipole nanoantenna-based wireless link system; KPFM signal scale bar: ±0.5 V. (e) 3D AFM image of channel SPP waveguide with an identical cross section to the waveguides in a−d and 3 μm length. (f) KPFM under optical illumination analysis of the channel SPP waveguide link; KPFM signal scale bar: ±4.7 V; inset (b, d, f): zoom in to the respective waveguide channel. Scale bar: 1 μm.

DOI: 10.1021/acs.nanolett.7b00266
Nano Lett. XXXX, XXX, XXX−XXX

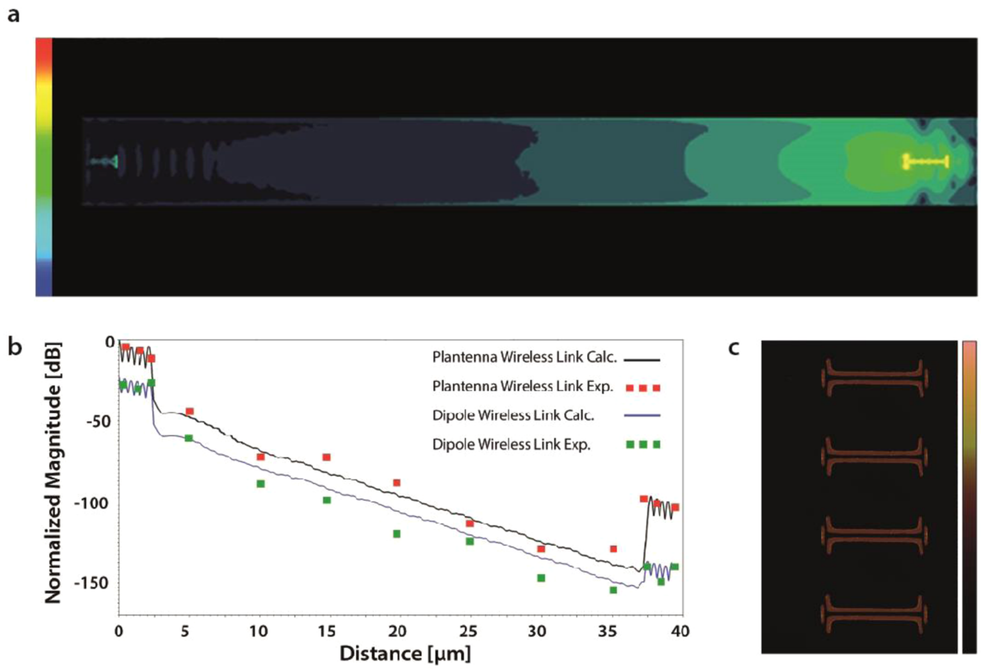

Figure 5. Performance analysis for ultralong propagation distances. (a) Numerically calculated near field image, showing the complete Plantenna-based wireless transfer link with distance of 35 μm between the transmitting and receiving sides. (b) Performance comparison between Plantenna and dipole based wireless links for 35 μm, showing a 30 dB better performance of the Plantenna configuration. (c) 3D AFM image of a three-element Plantenna based transceiver phased array. Scale bar: 200 nm.

the channel which is highlighted in the inset. Figure 4c shows the AFM topography of a wireless link based on dipole nanoantennas, which was recently proposed as an approach for plasmonic energy transfer;[18] the corresponding KPFM image is presented in Figure 4d with a voltage scale bar of ±0.5 V.

We observe plasmon excitation at the transceiver; however, significantly less noticeable intensity is measured at the receiver waveguide (see inset) compared with the Plantenna based architecture. Figure 4e shows a 3D AFM image of a Plantenna integrated with a similar waveguide of 3 μm length, implementing a direct nanoplasmonic link. Unlike the wireless links, the waveguide exhibits much higher propagation loss since it directly propagates tightly confined plasmons that interacts with the metals in their entire guided route.[18] A KPFM map of the direct link is shown in Figure 4f (scale bar ±4.7 V), where the zoom in to the different channel regions is presented in the insets. As seen in the right inset, channel SPPs are excited by the Plantenna and propagate through the waveguide. However, the huge propagation loss makes the waveguide SPPs decay significantly and being practically unobservable after propagating for only 2.5 μm, as seen in the left inset of Figure 4f. This reconfirms the critical, huge losses exhibited in gap plasmon waveguides with nanoscale channels, which hamper their real life applicability. Figure 5a shows the calculated electric near field for a Plantenna based communication nanosystem with a 35 μm distance between the transmitter and receiver. Even for this high separation, plasmon excitation is clearly observed in the receiving device. Dipole nanoantenna is the most popular form of compact couplers to channel waveguide, enabling us to achieve 200 times higher efficiency compared with the case of directly illuminating a base waveguide.[3,4,6,7,10,16] Other types of couplers may use nano-focusing approaches[15] or more complex coupling devices like a Yagi nanoantenna.[19] However, these devices are diffraction limited and cause only marginal improvement compared with the dipole coupler. A comparison between Plantenna and dipole based systems with 35 μm separation is shown in Figure 5b, presenting the normalized near field along a line that connects the transmitter and receiver passing through the centers of both waveguides. The continuous black and blue charts represent the calculated results of a Plantenna and dipole wireless systems, respectively, as the discrete red and green squared dots are the corresponding experimental results. High field values are observed in both Tx and Rx ends, attributed to plasmon enhancement by the nanoantennas. As expected, the field is attenuated linearly when propagates through the SiO_2 substrate.

A quantitative comparison between Plantenna and dipole systems is performed by comparing the SPP magnitude at both receiver waveguides, which serve as input for remote nano-plasmonic circuits[4,12,20] or can be probed by photoelectric detectors. Since both systems are excited with identical sources and use similar plasmon waveguides, this approach is equivalent to calculating the ratio between the wave power of the SPP at the receiver waveguide and the laser source. As seen in Figure 5b, the Plantenna based nanosystem outperforms the dipole configuration by more than 30 dB. Note that from nano-fabrication considerations we use Plantenna with identical dimensions through all of the experiments herein. However, the additional significant efficiency improvement can be achieved using a structural optimization of the different Plantennas as we recently reported.[5] The Plantenna nanosystem can be used to wirelessly transfer optical nanoplasmonic information for macroscale distances using a phased array[21−24] configuration as shown in Figure 5c. By fabricating an array of identical transceivers spaced by $\lambda_0/2$ (λ_0 is the free space wavelength), the emitted surface waves coupled from all of the transceivers can be coherently combined on the surface. Based on the well-known Friis principle,[18,25,26] the phased array architecture enables propagation distances which are linearly scalable with

DOI: 10.1021/acs.nanolett.7b00266
Nano Lett. XXXX, XXX, XXX−XXX

the number of transceivers, paving the way toward efficient wireless nanoplasmonic data and energy transfer for millimeter distances and beyond.

In conclusion, we designed, fabricated, and experimentally characterized a novel high-efficiency nanosystem, capable to wirelessly transfer deeply confined optical plasmon polaritons for chip−scale distances. Our system is architectured for the efficient conversion of nanoscopic SPPs to propagating surface waves and to re-excite SPPs from these surface waves at significantly remote distances. We demonstrate the transmission of optical SPPs in channel waveguides with a cross section of only 20 nm × 20 nm, for distances which are 3 orders of magnitude larger than the plasmon wavelength. On the basis of the Plantenna, a new generation of high-performance nanoantennas with no RF equivalents, our nanosystem hugely outperforms both direct and wireless links based on dipole nanoantennas by more than 30 dB. For the first time, we use a unique combination of scanning probe microscopies to create complete real-space near-field mapping of a long-range nanoplasmonic wireless link at a high spatial resolution. This nanoimaging amalgamation provides valuable synergy needed for mapping both nanoscopic plasmon polaritons as well as macroscopically propagating surface waves. In the quest for reconciling the dimensional mismatch between diffraction-limited photonics and integrated electronics, our results enable new horizons for high integration densities of optical functionalities and interconnects. By using phased array configuration and utilizing degrees of freedom in polarization, frequency and code domains, inter- and intra-chip communications based on ultrafast nanoscale light waves as information carriers can now achieve record performances in terms of speed distance and size. The presented approach of hybridizing Plantenna and channel plasmon waveguides as nanotransceivers is immediately applicable for exploring long-range interaction between single and multiple quantum emitters, while our nanoimaging methodology enables enhanced understanding of exciting near-field phenomena at the nanoscale.

Methods. *AFM and KPFM Measurements.* All measurements were performed at room temperature and free ambient conditions (no vacuum), using a Dimension Icon AFM system with a NanoScope V controller (Bruker). For both AFM and KPFM measurements, we used NanoWorld probes SSS-NCH (SuperSharpSilicon, Noncontact/Tapping mode, High resonance frequency), with a typical diameter of 2 nm, resonance frequency of 320 kHz, and spring constant of 42 N/m. Typically, voltages of 2 V, AC capacitance frequencies of 880 MHz, lift heights of 30−50 nm, and line rates of 0.1 kHz were employed. To map the CPD of the sample, we apply both AC voltage (VAC) and DC voltage (VDC) to the AFM tip. VAC generates oscillating electrical forces between the AFM tip and sample surface, and VDC nullifies the oscillating electrical forces that originated from CPD between tip and sample surface.

Optical Near-Field Measurements. The optical characterization of the plasmonic structures was performed by a MultiView 2000 scanning probe microscope/NSOM system (Nanonics Imaging Ltd.). The SPM head was placed on the stage of an Olympus dual microscope while remaining the optical axis free from above and below. Such a configuration allowed us to bring the cantilevered NSOM tip to the desired position on the sample under an upper objective of 50×. The sample was illuminated with a Liconix diode laser of 785 laser CW light from the bottom and focused on a sample with a 50× objective. We used the bottom piezo scanner of the scanning head to place the desired structures of the sample very accurately relatively to the incoming light of the laser from below. The scan was performed with upper piezo scanner allowing moving only the NSOM tip while the sample remains still. The collection of near field light distribution on the surface was performed in tapping mode with a 200 nm aperture NSOM tips based tuning fork produced by Super Tips (Nanonics Imaging Ltd.). The signal was transmitted through a multimode optical fiber onto an APD. The AFM and NSOM images were collected simultaneously during the scan, allowing to monitor the topography of the desired structure and to correlate it with the near-field optical signal that comes from any particular feature.

Numerical Simulations. The numerical results are obtained by using the software package ANSYS HFSS V15, the industry-standard simulation tool for 3D full-wave electromagnetic field simulation. HFSS solves Maxwell's equations via the finite element method (FEM) using an adaptive mesh refinement process for tailored accuracy requirements. The field's solutions are calculated with the metallic (Ag) plasmonic structures being deposited on a homogeneous SiO_2 substrate. The nanoantenna is illuminated by optical sources at 474 THz (wavelength of 633 nm), which are modeled as focused Gaussian beams with 1 μm characteristic diameter. The electric field is polarized in parallel with the dipole direction, as the wave vector $\mathbf{K}$ is perpendicular. A selectively dense meshing is assigned in the metallic and waveguiding regions, with a maximum cell size of 1 nm and 750 000 FEM tetrahedral cells. To provide maximum accuracy, the model is terminated as following: the interface with free space is bounded by perfectly matched layer (PML) absorbing boundary conditions (ABC), while the metallic and SiO_2 termination are done via layered impedance (LI) ABC. The minimum number of adaptive meshing iterations was set to 12, with a convergence condition of 1% maximum energy variance between adjacent iterations.

Fabrication. SiO_2/Si sample was spin-coated with poly(methyl methacrylate) (PMMA 950 A2) electron-beam resist providing thickness of 100 nm. The samples coated with PMMA were subsequently baked for 120 s on a hot plate at 180C. The desired pattern was exposed in the PMMA layer using a CRESTEC CABLE-9000C high-resolution electron-beam lithography system using different doses to control line and gap width. Then the samples were developed for 90 s using methyl isobutyl ketone (MIBK) and rinsed with IPA. The samples were subsequently exposed to Ar plasma to etch 10 nm in order to remove leftovers from the pattern, sputtered using BESTEC 2″ DC magnetron to deposit 2 nm Cr and 18 nm Au, and then immersed in 180 Khz ultrasonic bath with NMP for 3 h for resist liftoff.

■ AUTHOR INFORMATION

Corresponding Author

*E-mail: moshik.cohen80@gmail.com.

ORCID

Moshik Cohen: 0000-0002-7519-9742

Author Contributions

M.C. carried out the theoretical design and analysis, designed the studies, performed the experiments, and wrote the manuscript. Z.Z. and R.S. participated in writing the manuscript and designing the study.

DOI: 10.1021/acs.nanolett.7b00266
Nano Lett. XXXX, XXX, XXX−XXX

Notes

The authors declare no competing financial interest.

■ ACKNOWLEDGMENTS

M.C. acknowledges Olga Girshevitz Yafit from Bar-Ilan Institute for Nanotechnology & Advanced Materials (BINA), for the support in fabricating the reported structures.

■ REFERENCES

(1) Schuller, J. A.; Barnard, E. S.; Cai, W.; Jun, Y. C.; White, J. S.; Brongersma, M. L. *Nat. Mater.* **2010**, *9* (3), 193−204.

(2) Brongersma, M. L.; Shalaev, V. M. *Science* **2010**, *328* (5977), 440−441.

(3) Cohen, M.; Shavit, R.; Zalevsky, Z. *Sci. Rep.* **2015**, *4*, 04096.

(4) Cohen, M.; Zalevsky, Z.; Shavit, R. *Nanoscale* **2013**, *5* (12), 5442−5449.

(5) Cohen, M.; Shavit, R.; Zalevsky, Z. *Sci. Rep.* **2015**, *5*, 17562.

(6) Cohen, M.; Shavit, R.; Zalevsky, Z. In *Planar Waveguides and other Confined Geometries*; Marowsky, G., Ed.; Springer Series in Optical Sciences; Springer: New York, 2015; pp 45−66.

(7) Dionne, J. A.; Sweatlock, L. A.; Atwater, H. A.; Polman, A. *Phys. Rev. B: Condens. Matter Mater. Phys.* **2006**, *73* (3), 035407.

(8) Bozhevolnyi, S. I.; Volkov, V. S.; Devaux, E.; Laluet, J.-Y.; Ebbesen, T. W. *Nature* **2006**, *440* (7083), 508−511.

(9) Dregely, D.; Lindfors, K.; Lippitz, M.; Engheta, N.; Totzeck, M.; Giessen, H. *Nat. Commun.* **2014**, *5*, 4354.

(10) Cohen, M.; Abulafia, Y.; Shavit, R.; Zalevsky, Z. *ACS Nano* **2017**, *11*, 3274.

(11) Carmeli, I.; Cohen, M.; Heifler, O.; Lilach, Y.; Zalevsky, Z.; Mujica, V.; Richter, S. *Nat. Commun.* **2015**, *6*, 7334.

(12) Cohen, M.; Shavit, R.; Zalevsky, Z.; Abulafia, Y. In *CLEO: 2014*; OSA Technical Digest (online); Optical Society of America, 2014; p JTu4A.135.

(13) Lu, H.; Liu, X.; Wang, G.; Mao, D. *Nanotechnology* **2012**, *23* (44), 444003.

(14) Wang, S.; Zhan, Q. *Sci. Rep.* **2016**, *6*, 29626.

(15) Choo, H.; Kim, M.-K.; Staffaroni, M.; Seok, T. J.; Bokor, J.; Cabrini, S.; Schuck, P. J.; Wu, M. C.; Yablonovitch, E. *Nat. Photonics* **2012**, *6* (12), 838−844.

(16) Wen, J.; Romanov, S.; Peschel, U. *Opt. Express* **2009**, *17* (8), 5925−5932.

(17) Andryieuski, A.; Zenin, V. A.; Malureanu, R.; Volkov, V. S.; Bozhevolnyi, S. I.; Lavrinenko, A. V. *Nano Lett.* **2014**, *14* (7), 3925−3929.

(18) Alù, A.; Engheta, N. *Phys. Rev. Lett.* **2010**, *104* (21), 213902.

(19) Solís, D. M.; Taboada, J. M.; Obelleiro, F.; Landesa, L. *Opt. Express* **2013**, *21* (2), 2369−2377.

(20) Dionne, J. A.; Sweatlock, L. A.; Sheldon, M. T.; Alivisatos, A. P.; Atwater, H. A. *IEEE J. Sel. Top. Quantum Electron.* **2010**, *16* (1), 295−306.

(21) Abediasl, H.; Hashemi, H. *Opt. Express* **2015**, *23* (5), 6509−6519.

(22) Cohen, E.; Ruberto, M.; Cohen, M.; Degani, O.; Ravid, S.; Ritter, D. *IEEE Trans. Microwave Theory Tech.* **2013**, *61* (3), 1359−1375.

(23) Sun, J.; Timurdogan, E.; Yaacobi, A.; Hosseini, E. S.; Watts, M. R. *Nature* **2013**, *493* (7431), 195−199.

(24) Maguid, E.; Yulevich, I.; Veksler, D.; Kleiner, V.; Brongersma, M. L.; Hasman, E. *Science* **2016**, *352*, 1202.

(25) Choi, H. S.; Kang, S. Y.; Cho, S. J.; Oh, I.-Y.; Shin, M.; Park, H.; Jang, C.; Min, B.-C.; Kim, S.-I.; Park, S.-Y.; Park, C. S. *Sci. Rep.* **2015**, *4*, 5486.

(26) Yang, Y.; Li, Q.; Qiu, M. *Sci. Rep.* **2016**, *6*, 19490.

DOI: 10.1021/acs.nanolett.7b00266
Nano Lett. XXXX, XXX, XXX−XXX